Journal of Materials Chemistry A

Accepted Manuscript

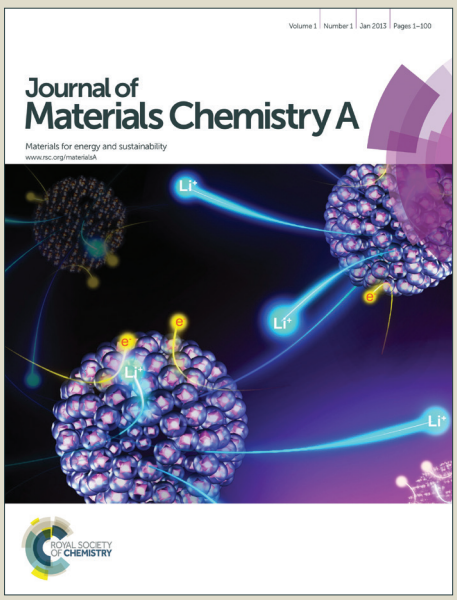

ROYAL SOCIETY OF CHEMISTRY

www.rsc.org/materialsA

Cite this: DOI: 10.1039/c0xx00000x

www.rsc.org/xxxxxx

ARTICLE TYPE

ZnO Nanorods/ZnSe Heteronanostructure Arrays with a Tunable Microstructure of ZnSe Shell for Visible Light Photocatalysis

Zhengcui Wu,* Huan Wang, Yejing Xue, Baoer Li and Baoyou Geng*

Received (in XXX, XXX) Xth XXXXXXXXX 200X, Accepted Xth XXXXXXXXX 200X

DOI: 10.1039/b000000x

The surface modification of the semiconductors is an important strategy for tuning solar-driven photocatalytic activity. Herein, the high visible light photocatalytic activity of ZnO nanorods/ZnSe heteronanostructure arrays with a tunable microstructure of ZnSe shell are achieved by the liquid chemical conversion with ZnO nanorods array on zinc foil. Through inducing by ammonia molecules, the secondary ZnSe shell with nanoparticles, nanorods and nanosheets is engineered by the oriented attachment of small ZnSe nanoparticles. By virtue of the synergic advantages of enhanced visible light adsorption capability and effective separation of electron-hole pairs benefited from coupling with ZnSe nanostructures, the ZnO nanorods/ZnSe heteronanostructure arrays exhibit significantly promoted visible light driven photocatalytic activities as well as shell microstructure dependent photocatalytic performance.

Introduction

The efficient utilization of solar energy for photocatalytic degredation organic pollutants has attracted great research interest due to the increasing awareness of the inverse impacts of industrialization on our environment.[1-3] In view of the omnipresent existence of semiconductor minerals, e.g. transition metal oxides and sulfides, the photodegradation of environmental organic compound, particularly the organic pollutants in water became possible through constructing stable and efficient photochemical systems, which has emerged as a promising technique for disposing wastewaters containing low-concentration organic dye pollutants.[3] ZnO, an important wide and direct band-gap semiconductor (3.37 eV for bulk ZnO), is generally accepted as a promising photocatalyst due to its low cost, high catalytic efficiency and environmental sustainability.[4,5] However, ZnO can primarily make use of UV light with about 4% of the total sunlight reaching the earth, hardly absorb visible light accounting for about 43% of the solar spectrum, which restricts its potential as a solar-driven photocatalyst. Moreover, the practical applications are still handicapped by its poor photostability due to the photoinduced dissolution in photocatalytic processes.[6] Thus, the key to promotion ZnO-mediated photocatalytic degradation is to modify the ZnO surface with another material for a high solar utilization efficiency and enhancing the separation of photogenerated charges. Coupling narrow band gap semiconductor with ZnO is regarded as an efficient strategy to extend photoabsorption to the visible range and reduce the inclination of charge recombination.[7-12] Although ZnO/CdX (X = S, Se, or Te) heterostructures have been described for this purpose,[13-15] the carcinogenic risks of many Cd-related compounds prevent their real applications in photocatalysis. ZnSe is an environmentally friendly narrow band gap semiconductor (2.67 eV for bulk ZnSe), of which the valence and conduction bands are aligned in a staggered manner relative to those of ZnO, being candidate for producing type II ZnO heterostructures, offering great potential to improve the ZnO-mediated photocatalysis by more effective utilization the sun as a free green light source and promoting the separation of photogenerated electron-hole pairs.

Substantial efforts have been devoted to prepare ZnO-ZnSe heterostructures, including chemical vapor deposition[16a,b] and solution-phase synthesis,[16c-g] of which various ZnO/ZnSe heterostructures such as nanowire arrays,[16a-c] core/sheath nanorod arrays,[16d] porous nanocomposites,[16e] three-dimensional heterostructures,[16f] ZnO-decorated ZnSe nanorods[16g] have been obtained. However, none of the developed methods so far provides rational control over novel architectures of ZnSe shell apart from the simple single- or poly-crystalline ZnSe shell covered on primary ZnO nanostructures. Moreover, it is still not sufficient to disclose the important correlation between the microstructure and the photocatalytic property. Therefore, it seems desirable to explore facile and rational synthetic strategies for intriguing ZnO/ZnSe heteronanostructures with various novel architectures of ZnSe shell for promoting and extending the chemical functionalities and physical properties. Herein, we present a facile liquid-phase synthetic route to yield ZnO nanorods/ZnSe heteronanostructure arrays with a tunable microstructure of ZnSe shell via the liquid chemical conversion with ZnO nanorods on zinc foil, of which the nanoparticles, nanorods and nanosheets of ZnSe shell can be fabricated by increasing the concentration of ammonia, and the ammonia molecules are intercalated into the final ZnSe nanosheets shell with high concentration of ammonia, which can be subsequently released by calcination in N_2 atmosphere with morphology maintained. Importantly, this approach allows one to deliberately tailor the ZnSe shell with novel architectures, providing an opportunity to explore the correlative properties including

photocatalysis. The experiments of photodegradation Rhodamine B reveal that the fabricated ZnO nanorods/ZnSe heteronanostructure arrays show excellent visible light photocatalytic activities and recycled stability, which is very attractive for real applications in photocatalysis.

Experimental Section

Sample preparation

All chemicals were of analytical grade and used as received without further purification.

Synthesis of ZnO Nanorods (ZnO-NRs) Array on Zinc Foil: The synthesis was according to our recent report.[17] In a typical synthesis, a washing cleaned zinc foil (99.9% 1×3 cm) was inserted into the solution with 4 mL of 1, 6-hexanediamine and 40 mL of distilled water in a teflon-lined stainless steel autoclave of 50 mL capacity, which was then heated at 180 °C for 5 h and cooled to room temperature naturally. The white precipitate covered on zinc foil was washed with distilled water and ethanol several times to remove residual ions and dried at 50 °C for 6 h.

Synthesis of ZnO Nanorods/ZnSe Heteronanostructure Arrays on Zinc Foil: The synthesis was taken out as following: 0.01 g of Se power was added into the solution with different volume of ammonia and distilled water keeping total volume of 40 mL under constant stirring in a 100 mL glass reaction bottle, then 0.01 g of $NaBH_4$ was added. After 30 min of agitation, the zinc foil covered by ZnO-NRs array was inserted, and the mixture was heated at 90 °C for 8 h. The resulting zinc foil covered with hairy precipitate was washed with distilled water and ethanol several times, then dried at 50 °C for 6 h for further characterization. For arrays of ZnO nanorods/ZnSe nanoparticles (ZnO-NRs/ZnSe-NPs), ZnO nanorods/ZnSe nanorods (ZnO-NRs/ZnSe-NRs) and ZnO nanorods/ZnSe nanosheets (ZnO-NRs/ZnSe-NSs) precursor, the volume of ammonia was 5 mL, 15 mL and 20 mL, respectively. And the ZnO-NRs/ZnSe-NSs array was subsequently obtained by calcination of ZnO-NRs/ZnSe-NSs precursor array in a porcelain boat at 350 °C for 1 h in N_2 atmosphere with the heating rate of 5 °C/min from room temperature to 350 °C.

Characterization

Powder X-ray diffraction patterns (XRD) were recorded on a Rigaku TTRIII diffraction system with high-intensity Cu Kα radiation. Field-emission scanning electron microscope (FESEM) images were obtained by a Hitachi S-4800 scanning electron microscope. Transmission electron microscopy (TEM) analysis was taken on a JEOL 2010 operated at an accelerating voltage of 200 kV. UV-visible diffuse reflectance spectra were carried out on a Shimadzu UV-2450 spectrophotometer using magnesium oxide as a standard. Photoluminescence (PL) spectra were obtained on a LS-55 (Perkinelmer, USA) with a Xe laser as the excitation light source at 380 nm. Brunauer-Emmett-Teller (BET) nitrogen adsorption-desorption was measured using a Micromeritics ASAP 2020 accelerated surface area and porosimetry system.

Photocatalytic Experiments

Photocatalytic activities of the as-synthesized ZnO-NRs/ZnSe heteronanostructure arrays were evaluated by measuring the photodegration of Rhodamine B (RhB) as a representative dye pollutant under visible light irradiation. The ZnO-NRs/ZnSe heteronanostructure array was cut into 1×1.5 cm and placed in the bottom of a vial (25×40 mm) containing 5 mL of 10^{-5} M RhB aqueous solution and placed in the dark for 1 h to reach the adsorption/desorptiom equilibrium on the catalyst surface. Then, visible light irradiation was carried out using a 300 W Xe lamp with a cutoff filter (λ > 420 nm) (PLS-SXE300/300UV, Trusttech, Beijing). At a given time interval of 20 min, the absorbance spectra of the solution was recorded on a UV-vis spectrophotometer (Shimadzu UV-2550), from which the concentration of RhB was measured by monitoring its characteristic absorption at 554 nm.

Photo-electrochemical measurements

To conduct the photo-electrochemical measurements, the products were fabricated into films on ITO glasses. The detailed fabrication process of the films was carried out as follows: The products obtained by scratching the foil were initially dispersed in ethanol to obtain a concentration of 0.3 $mg \cdot mL^{-1}$, then 5 mL ethanol dispersion of the products was uniformly spin-dropped on the 1.5×1.5 cm ITO-coated glass at 500 r.p.m. for 30 s by a desktop spin coater (KW-4A, made by the Chinese Academy of Sciences), afterwards, the ITO-coated glasses were heated at 60 °C for 30 min to volatilize the solvent. The photo-electrochemical test systems were composed of a standard three-electrode configuration with the product deposited on ITO-coated glass as the working electrode, the Pt plate (1×1 cm) and the Ag/AgCl electrode as the counter and the reference, respectively, which were immersed in 0.5 $mol \cdot L^{-1}$ Na_2SO_4 solution by purged with nitrogen for 10 min prior to the measurement. The photo-electrochemical properties were measured on electrochemical station (CHI660B, Shanghai Chenhua Limited, China) in ambient conditions under illumination using a 300 W Xe lamp with a cutoff filter (λ > 420 nm). The potential was swept from − 0.3 to + 0.7 V (versus Ag/AgCl) at a sweep rate of 10 $mV \cdot s^{-1}$.

Results and Discussion

The crystalline phase of ZnO-NRs/ZnSe-NPs heterostructure array was first identified by XRD study. As shown in Figure 1, the additional diffraction peaks at 27.3° (111), 45.3° (220) and 53.6° (311) clearly indicate the existence of the cubic phase of ZnSe (JCPDS No. 37-1463) along with the diffraction peaks

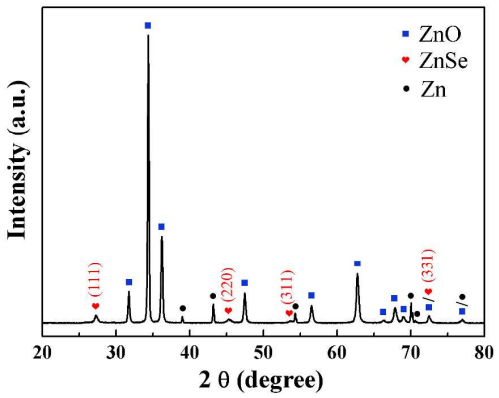

Figure 1. XRD pattern of the as-synthesized ZnO-NRs/ZnSe-NPs heterostructure array on zinc foil.

attributed to the wurtzite-type ZnO-NRs on zinc foil. Therefore, the XRD pattern confirms the formation of the ZnSe phase on ZnO-NRs. The product was also observed by the FESEM with energy dispersive X-ray spectroscopy (EDX). Figure 2a, b show the low- and high-magnification FESEM images of the nanorod-like heteronanostructure with an average diameter of about 250 nm and a length of several micrometers with rough surfaces. Compared with the needle-like ZnO-NRs with smooth surfaces after the first hydrothermal treatment (Figure S1), the result suggests the secondary nanoparticles are uniformly assembled on the whole surface of primary ZnO-NRs. The compositional information of the EDX in Figure 2c showed Se element is present with the atomic percent of 11.47% along with Zn and O elements, providing powerful evidence that Se element is successfully incorporated into the ZnO-NRs surface. The ZnSe-NPs shell grown on ZnO-NRs is further confirmed by TEM measurements. The TEM image of an individual nanorod in Figure 2d shows the nanoparticles with average size of 35 nm are attached on the ZnO nanorod and the coverage of nanoparticles shell was gradually decreased from the top to bottom of the ZnO nanorod, further offering evidence for the formation of ZnO-NRs/ZnSe-NPs heteroarchitecture. The HRTEM image in Figure 2e along both sides of the interface clearly displayed two different crystal parts, where one set of the planar spacing about 0.26 nm corresponded to the (002) plane of hexagonal wurtzite-type ZnO, another set of the fringes' spacing measured ca. 0.33 nm corresponded to the (111) lattice spacing of cubic ZnSe, indicating that the ZnSe nanoparticles shell was indeed grown over the ZnO nanorod core. The HRTEM image in Figure 2f further reveals the good crystalline nature of ZnSe nanoparticles shell. It was found the size, uniformity of coverage and content of secondary ZnSe nanoparticles on ZnO nanorods can be tailored by varying amounts of $NaBH_4$, ammonia and the reaction time (Figure S2).

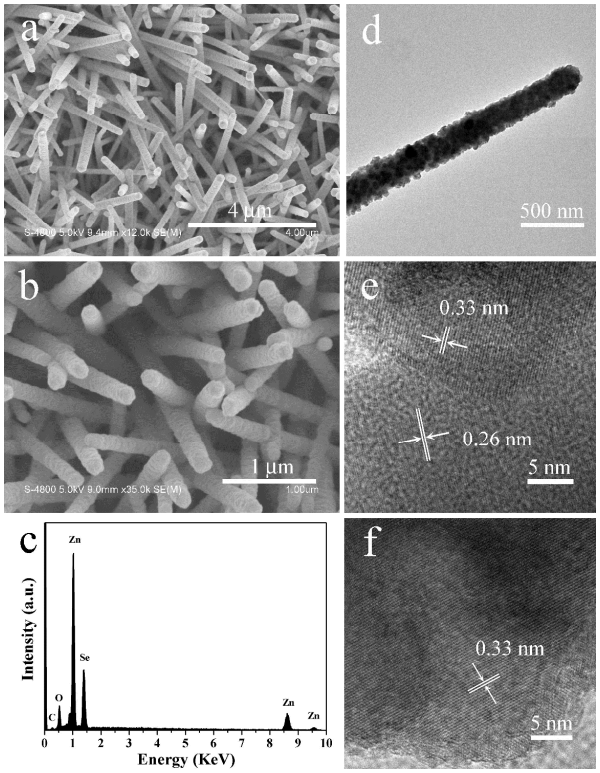

Figure 2. Morphological and structural characterization of the ZnO-NRs/ZnSe-NPs heterostructure array. (a, b) The FESEM images with low- and high-magnification, respectively; (c) The EDX spectrum; (d) The TEM image of an individual ZnO-NRs/ZnSe-NPs heterostructure; (e) The HRTEM image of the junction, showing the characteristic lattice planes of ZnO and ZnSe, respectively; and (f) The HRTEM image of the ZnSe nanoparticle shell, showing its high crystallity.

At 15 mL of ammonia, the obtained heteronanostructure array is small hierarchical ZnSe nanorods covered on ZnO nanorods as shown in Figure 3a, b. Careful observation can find that the ZnSe nanorods were assembled by tiny nanoparticles. The EDX spectrum in Figure 3c shows the atomic percent of Se is 25.18%, indicating more ZnSe were formed, which can be attributed to the higher concentration of ammonia promoted the dissolution and conversion of ZnO nanorods. The corresponding XRD pattern shown in Figure 3d indicates that the as-synthesized sample is still composed of ZnO and ZnSe phases on zinc foil. The TEM image in Figure 3e further showed the shell is assembled by small nanorods and the HRTEM image in Figure 3f taken at the edge of the nanorod shell shows its polycrystalline nature, clarifying the nanorod was assembled by tiny nanoparticles. The study focused on the concentration of $NaBH_4$ and the reaction time reveals their important roles on the formation of secondary ZnSe nanorods shell (Figure S3).

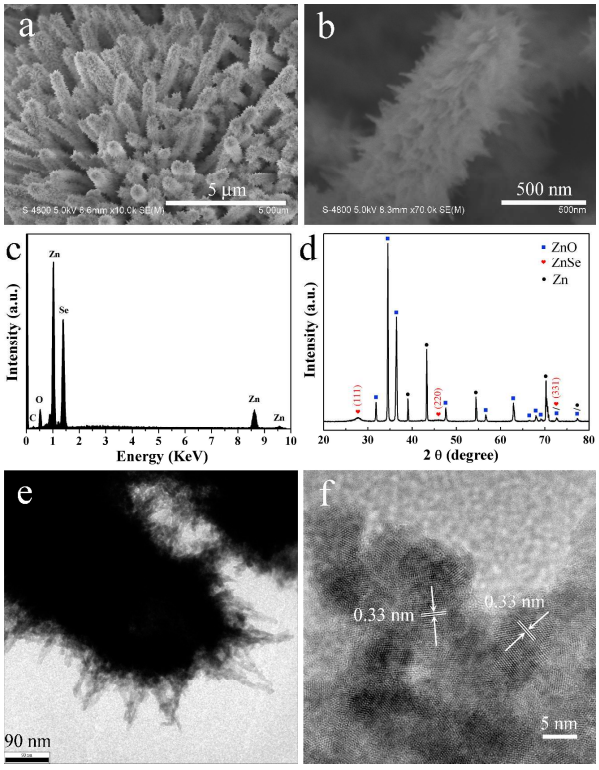

Figure 3. Morphological and structural characterization of the ZnO-NRs/ZnSe-NRs hierarchical heterostructure array. (a, b) The FESEM images with low- and high-magnification, respectively; (c) The corresponding EDX spectrum; (d) The XRD pattern; (e) The TEM image of a part of an individual ZnO-NRs/ZnSe-NRs, clearly showing the nanorod shell; and (f) The HRTEM image of the nanorod shell, showing its polycrystalline nature.

Further increased ammonia to 20 mL produced the nanosheet-

like shell array as the FESEM images shown in Figure 4a, b. The EDX spectrum in Figure 4c shows that the atomic percent of Se is 25.54%. Simultaneously, the element of N was appeared with high atomic percent of 25.23%, indicating N element is probably incorporated into the product. The corresponding XRD pattern in Figure 4d cannot be indexed to pure ZnSe phase except for the diffraction peaks related to ZnO-NRs and Zn foil. Moreover, some diffraction peaks related to ZnO-NRs were weakened or disappeared, illustrating that more ZnO nanorods are dissolved and converted at higher concentration of ammonia. The TEM image in Figure 4e clearly shows the shell was composed of nanosheets and the HRTEM image in Figure 4f taken from the nanosheet can be indexed to (111) lattice spacing of cubic ZnSe, where the lattice fringes were not continuous, indicating the nanosheets should be assembled with tiny nanostructure units by oriented attachment. The FESEM images of the product after calcination in Figure 5a and b exhibit the nanosheetlike shell was remained. The EDX spectrum in Figure 5c did not detect N element anymore. The XRD pattern in Figure 5d indicates the diffraction peaks are in good agreement with the cubic phase of ZnSe apart from those of ZnO nanorods and Zn foil, demonstrating that the inserted small molecules are released by calcination. The TEM image in Figure 5e further shows the nanosheet shell was remained and the HRTEM image in Fig. 5f taken on the nanosheet displayed its polycrystalline nature, and the clear lattice fringes can also be indexed to (111) lattice spacing of cubic ZnSe. The further investigations on the concentration of $NaBH_4$ and the reaction time provided insight into their roles on the formation of nanosheet-like shell (Figure S4).

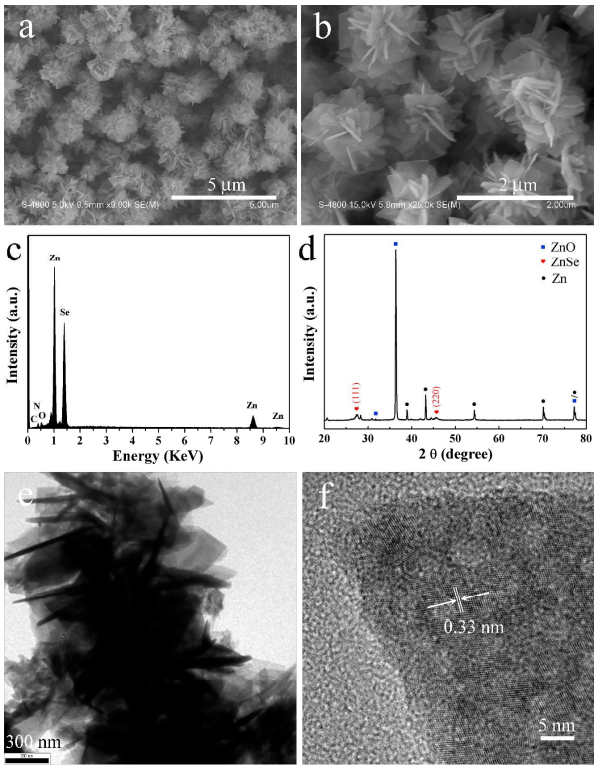

Figure 4. Morphological and structural characterization of the ZnO-NRs/ZnSe-NSs heterostructure precursor array. (a, b) The FESEM images with low- and high-magnification, respectively; (c) The EDX spectrum; (d) The XRD pattern; (e) The TEM image of a part of an individual ZnO-NRs/ZnSe-NSs precursor, clearly showing the nanosheetlike shell; and (f) The HRTEM image of the nanosheet shell, showing its polycrystalline nature.

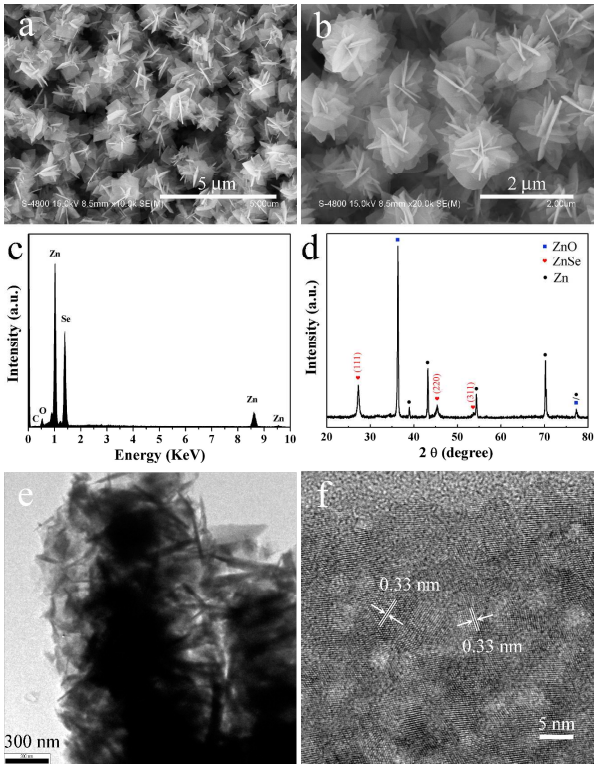

Figure 5. Morphological and structural characterization of the ZnO-NRs/ZnSe-NSs heterostructure array by calcination the ZnO-NRs/ZnSe-NSs precursor array. (a, b) The FESEM images with low- and high-magnification, respectively; (c) The EDX spectrum; (d) The XRD pattern; (e) The TEM image of a part of an individual ZnO-NRs/ZnSe-NSs; and (f) The HRTEM image of the nanosheet shell, showing its polycrystalline nature.

In this approach, the formation of ZnSe nanostructures on ZnO nanorods array is taken advantage of the selenization conversion with ZnO nanorods in the presence of the Se source. Under alkaline conditions of ammonia, hydroxyl anions slowly dissolved the surfaces of ZnO nanorods and released $Zn(OH)_4^{2-}$ near the surfaces of ZnO nanorods. And Se^{2-} anions released from the reduction of the Se power in $NaBH_4$ and ammonia at designed temperature then reacted with $Zn(OH)_4^{2-}$, producing ZnSe seeds covered on the ZnO nanorods. The ZnSe seeds can further grow into nanoparticles shell, or assemble into nanorods shell by oriented attachment at increased concentration of ammonia and further nanosheets shell with ammonia molecules inserted into the final structure with further increased ammonia concentration. Here, the critical factors that influence the microstructure of ZnSe shell are the concentrations of ammonia and $NaBH_4$, which codetermined the Se^{2-} concentration in the reaction system, providing growth-driving force for ZnSe nanocrystals. In addition, the ammonia molecules tend to be selectively adsorbed on the ZnSe nanocrystal surface through surface ions, which will induce the tiny nanocrystals assemble into nanorod-like and further nanosheet-like structure by oriented attachment with enough ammonia molecules adsorbed. Meanwhile, the ammonia molecules are intercalated the nanosheet-like structure. Undoubtedly, it is the high distribution density and the wide separation between the adjacent nanorods of these aligned needle-

like ZnO-NRs array that provides a good opportunity for uniform conversion of ZnSe nanostructures onto the large exposed surfaces of ZnO nanorods.[17,18] Moreover, the final heteronanostructure array on zinc foil has the advantage of not mixing with uncompletely dissolved reactant of selenium powder if any. Certainly, it still needs more systematic and in-depth study to make clear the exact functions of ammonia and $NaBH_4$ on the adjustment of ZnSe shell microstructure. Based on the experimental results, the formation mechanism of ZnO-NRs/ZnSe heteronanostructure arrays is schematically elucidated in Scheme 1.

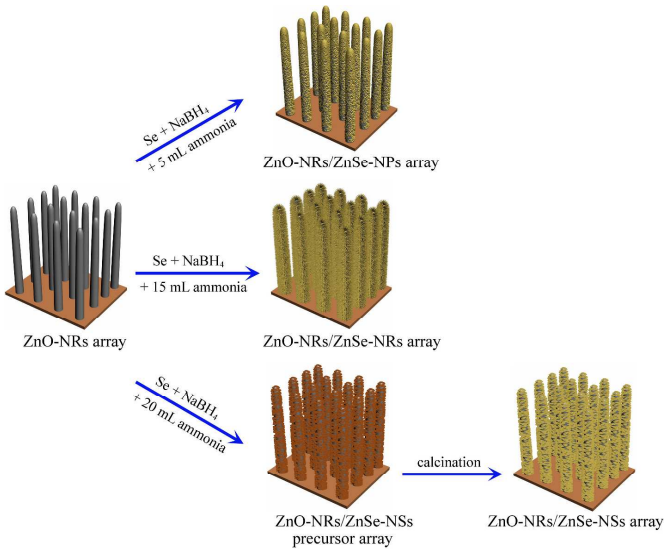

Scheme 1. Schematic image of the formation of ZnO-NRs/ZnSe heteronanostructure arrays on zinc foil.

The optical properties of the ZnO-NRs/ZnSe heteronanostructures were studied by the combined analyses of the UV-visible diffuse reflectance spectra and the photoluminescence (PL) spectra. As shown in Figure 6a, the spectrum of ZnO-NRs showed a strong UV adsorption band characteristic of the wide band gap materials of ZnO semiconductor along with a small absorption tail in the visible region. The ZnO-NRs/ZnSe heteronanostructures all displayed a strong absorption in the UV region as well as in the visible region, which can be ascribed to the visible light absorption of ZnSe nanocrystallites in the heterostructures. In addition, the ZnO-NRs/ZnSe-NSs heterostructure absorbed more visible light than the other two heterostructures, indicating it could generate more photoexcited charges in the visible light region that will facilitate the photodegradation of organic dye pollutant. By calculation from the UV diffraction reflection spectra in Figure 6a with the Tauc equation,[19,20] the optical band gaps of ZnO-NRs/ZnSe heteronanostructures were determined by the extrapolation of the Tauc plots (Figure S5). It can be seen that three ZnO-NRs/ZnSe heteronanostructures presented similarly optical band gaps at 3.24 to 3.30 eV and 2.63 to 2.73 eV, which are corresponding to the band gaps of ZnO and ZnSe, respectively. The PL spectra were examined to evaluate the recombination of photogenerated electrons and holes,[21,22] from which the migration, transfer and recombination process of photoexcited electron-hole pairs can be revealed. As shown in Figure 6b, all of the PL spectra possess two similarly independent peaks, where the sharper peaks at shorter wavelength region correspond to the near-band-edge emission while the broader peaks at longer wavelengths can be assigned to the defect-related emission. Slight blue shifts of the broad peaks at longer wavelengths for the heteronanostructures are observed, which may be related with the crystal perfection and the presence of defects that can strongly affect the photoluminescence features.[23] Moreover, the PL intensity of the heteronanostructures decreased after the ZnSe nanostructures are combined to ZnO nanorods, demonstrating the efficient charge separation.[24]

The photocatalytic degradation of organic dyes and toxic pollutants, which is greatly significant in environmental pollutant treatment, is a commonly used method to characterize the activity of photocatalysts. The photocatalytic activities of ZnO-NRs/ZnSe heteronanostructure arrays are evaluated under visible light irradiation using cationic dye Rhodamine B (RhB) as a representative dye pollutant in aqueous solution, and the relevant data for the ZnO-NRs array and without catalyst are also presented as contrast (Figure 7). The results showed the ZnO-NRs array and three kinds of ZnO-NRs/ZnSe heteronanostructure arrays all had a small quantity of adsorption for RhB molecules before light irradiation, of which the different adsorption amount may be attributed to the difference of the product's mass and surface area. Generally, the photocatalytic degradation of the dye was evaluated after its adsorption/desorption equilibrium on the catalyst surface. Thus, the photocatalytic degradation rate of RhB in the presence of ZnO-NRs/ZnSe-NSs reaches 96.0% after 120 min, while 87.6% with ZnO-NRs/ZnSe-NRs and 84.8% with ZnO-NRs/ZnSe-NPs array, but 5.6% with ZnO-NRs. The results also showed there was only slight degradation without catalyst (about 2.6%), indicating that the photoinduced self-sensitized photolysis can be ignored in comparison with the photocatalysis caused by the catalysts of the ZnO-NRs/ZnSe heteronanostructure arrays. The photocatalytic degradation of the arrays with same mass was also carried out (Figure S6). Clearly, the ZnO-NRs/ZnSe heteronanostructure arrays have much superior visible light photocatalytic activities than that of ZnO-NRs array. In addition, the photocatalytic activities of the ZnO-NRs/ZnSe heteronanostructure arrays vary with their microstructure, and the

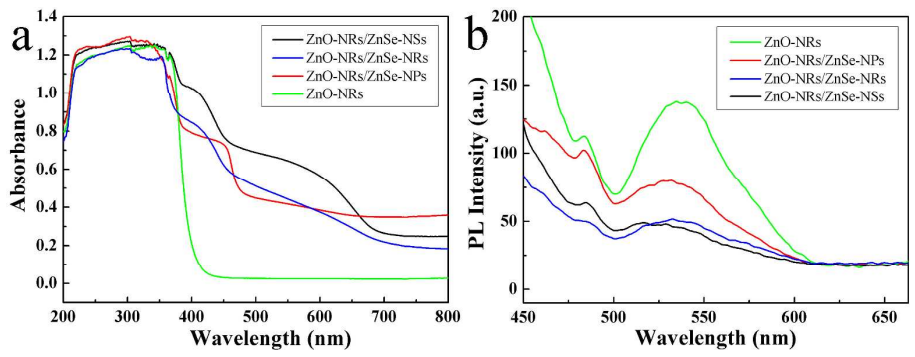

Figure 6. The optical properties of the ZnO-NRs/ZnSe heteronanostructures. (a) The UV-visible diffuse reflectance spectra; and (b) The PL spectra.

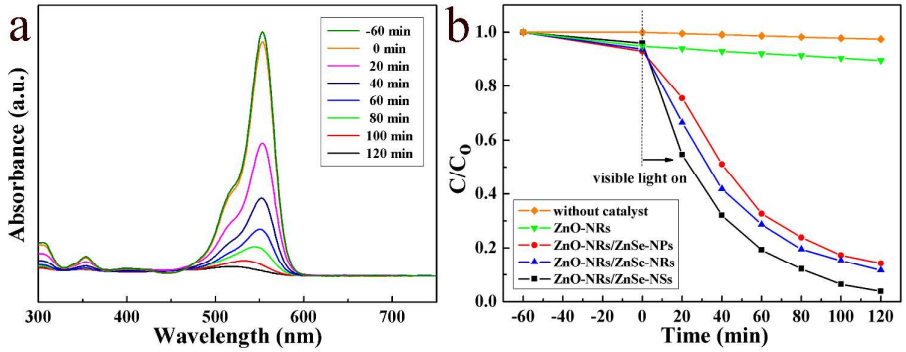

Figure 7. (a) UV-visible absorption spectra of photodegradation RhB aqueous solution with ZnO-NRs/ZnSe-NSs heterostructure array; and (b) Comparison of RhB photodegradation without catalyst, with ZnO-NRs array and three different ZnO-NRs/ZnSe heteronanostructure arrays.

ZnO-NRs/ZnSe-NSs heterostructure array has better photocatalytic performance than that of the other two heteronanostructures, which is probably due to the larger surface area and more surface atoms of the ZnSe nanosheet shell that improves reactive adsorption/desorption sites and visible light absorption for photocatalytic reactions.

The BET surface areas of three ZnO-NRs/ZnSe heteronanostructures were determined by the nitrogen sorption experiments (Figure S7). It showed the sample of ZnO-NRs/ZnSe-NSs heterostructure had the biggest BET surface area of 24.28 m^2/g, while 20.52 m^2/g with ZnO-NRs/ZnSe-NRs, and only 6.12 m^2/g with ZnO-NRs/ZnSe-NPs. The visible light photocatalytic activities of three ZnO-NRs/ZnSe heteronanostructure arrays with the same surface areas were conducted with different weights of catalysts inversely proportional to the specific surface areas by adjusting the size of the foil (Figure S8). The ZnO-NRs/ZnSe-NSs heterostructure array has the best photocatalytic activity among three heteronanostructures, implying the morphologies and exposed active crystal faces of the shell ZnSe nanostructure play an important role in the photocatalytic processes.[16f] In addition, the photocatalytic activity of ZnO-NRs/ZnSe-NPs was higher than that of ZnO-NRs/ZnSe-NRs, which may be due to its higher intrinsic catalytic activity.[25] The single-crystalline nature of ZnSe nanoparticles in ZnO-NRs/ZnSe-NPs heterostructure (see HRTEM image in Figure 2f) made less defects in the sample's surface, while ZnSe nanorods in ZnO-NRs/ZnSe-NRs heterostructure were composed of smaller nanoparticles (see HRTEM image in Figure 3f), thus formed more defects, which can become recombination centers of charge carriers. Moreover, the RhB photocatalytic activities of our ZnO-NRs/ZnSe-NSs heteronanostructure array should be better than that of the ZnO-decorated ZnSe nanorods,[16g] the only report about the ZnO/ZnSe heterostructure on photogradation of RhB up to now, considering the power of xenon lamp (500 W) and the amounts of catalyst and RhB aqueous solution (3 mg and 15 mL of 10^{-5} M, respectively) in that report. The high distribution density and the wide separation between the adjacent nanostructures of these ZnO-NRs/ZnSe heteronanostructure arrays can embody the structurally related photocatalytic activities to the maximum extent, effectively avoiding the possible damage of the microstructure and aggregation of the catalysts which are often faced by powder-form photocatalysts.

The photo-electrochemical measurements of ZnO-NRs/ZnSe heteronanostructures as well as ZnO-NRs have been carried out to evaluate the charge separation efficiency. The results were shown in Figure 8, of which all the samples exhibited small dark current densities, and three ZnO-NRs/ZnSe heteronanostructures presented much pronouced photocurrent density than that of ZnO-NRs under visible light irradiation. As the photocurrent observed under light illumination can reflect the number of charge carriers produced from the incident light,[26] the increased photocurrent density of the heterostructures can be attributed to the imporved visible light absorption by the ZnSe nanostructures, as shown in the UV-vis absorption spectra in Figure 6a, and a decrease in the probability of charge recombination by type II energy band alignment of ZnO and ZnSe.[16c] The maximum photocurrent density of the ZnO-NRs/ZnSe-NSs heterostructure can suggest the most visible light absorption ability and the most efficient photoelectric charge separation related to its microstructure from another point of view.

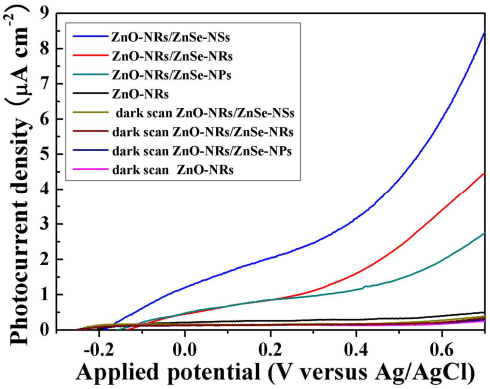

Figure 8. Photocurrent densities of ZnO-NRs and three ZnO-NRs/ZnSe heteronanostructures measured under a 300 W Xe lamp with a cutoff filter ($\lambda > 420$ nm) in 0.5 mol·L^{-1} Na_2SO_4 solution.

As is known a prerequisite for efficient photodegration pathway is the preadsorption of dye molecules on the photocatalyst surface in which excited dye molecules can inject electrons into the conduction band (CB) of the semiconductor.[27-29] Consequently, the charge properties of the surface of photocatalyst and dye molecule are critical for the adsorption. Because RhB is a kind of cationic dye molecules, to further clarify the photocatalytic process, an anionic dye of Methyl Orange (MO), was used as a probe molecule for comparison. Photodegradation rate of MO in the presence of ZnO-NRs/ZnSe-NSs heterostructure array only reaches about 21% after 120 min (Figure S9), demonstrating anionic dye of MO is difficult to be adsorbed on ZnO-NRs/ZnSe-NSs surface.[30] Therefore, the surface of our heteronanostructure catalyst may be rich of negative charges, which is probably come from the adsorption of OH^- during the synthetic process. Our work gives the first investigation on the photocatalytic gradation of different charged dye molecules with the synthesized

ZnO/ZnSe heteronanostructure, which is helpful to disclose the photocatalytic process more clearly.

To identify the dye photosensitization on enhancing the visible-light driven photodegradation of this color organics, a comparative experiment of the photocatalytic degradation of colorless organics of phenol was carried out with ZnO-NRs/ZnSe-NSs array under visible light irradiation. There was only about 4.1% by photodegradation after irradiation within the test period of 120 min (Figure S10). Therefore, it is reasonably believed that the indirect color dye photosensitization, i. e. dye degradation by the electron injection from dye to semiconductor plays a crucial role in the degradation of RhB under visible light irradiation.

In addition, to investigate the stability of the high photocatalytic behavior of the ZnO-NRs/ZnSe heteronanostructures, recycling experiments for the photocatalytic degradation of RhB were carried out taking ZnO-NRs/ZnSe-NSs array as an example (Table S1). The photodegradation efficiency of RhB solution changes from 96.0% in the first run to 93.5% in the tenth run, only decreased slightly over 10 consecutive cycles, exhibiting a good durability, which is especially attractive for its real application.

Under visible light irradiation, the semiconductor of ZnO or ZnSe can absorb a photon with energy equal to or higher than the band gap (Eg), and excite an electron from the valence band (VB) to the conduction band (CB),[2,31] producing reductive electrons on conduction band and oxidative holes on valence band. The RhB molecules can also be excited by harvesting visible light, and could effectively inject their photoexcited electrons into CB of the semiconductor they are adsorbed on, which can then initiate the adsorbed O_2 to generate active species of $\cdot O^{2-}$ for pollutant degradation. In addition, the valence and conduction bands of ZnSe are staggered with those of ZnO, of which the electrons on the conduction band of ZnSe could be injected to that of ZnO, and the holes could migrate from the valence band of ZnO to that of ZnSe, which promoted charge separation of the photogenerated electron-hole pairs before recombination. The holes can react with the H_2O molecules to produce $\cdot OH$ radicals and the electrons are usually scavenged by molecular O_2 to generate $\cdot O^{2-}$, which can initiate the subsequent radical reactions and lead to the facile oxidative degradation of RhB molecules into CO_2 and H_2O.[22] Therefore, it is the dye photo-sensitization, the surface adsorption behavior of cationic dye molecules, the enhanced visible light absorption of ZnSe nanostructures and the effective charged separation of the ZnO-NRs/ZnSe heterostructures that jointly contributed to the high photogradation performance of RhB. The electron-transfer process of ZnO-NRs/ZnSe heteronanostructure on photo-gradation of RhB is pictorially illustrated in Figure 9.

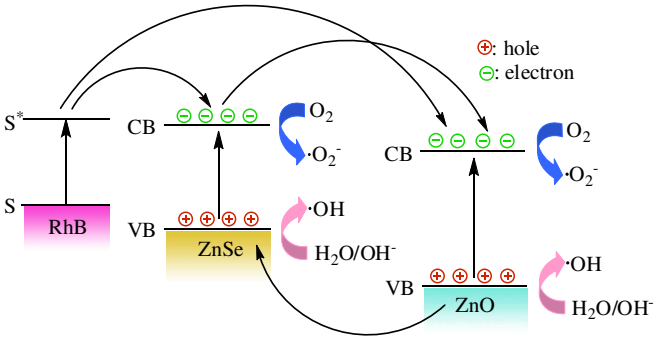

Figure 9. Schematic diagram of the electron-transfer process of ZnO-NRs/ZnSe heteronanostructure on photogradation of RhB.

Conclusions

This work provides a convenient liquid-phase chemical conversion route to generate ZnO-NRs/ZnSe heteronanostructure arrays on zinc foil with tunable microstructural ZnSe shell of nanoparticles, nanorods and nanosheets, not accessible by any of the known synthetic approaches before, and develops a better understanding for the correlation between the heteronano-architecture and photocatalytic activity. Benefiting from the dye photosensitization and the surface adsorption behavior of cationic dye molecules on the photocatalyst, the fabricated ZnO-NRs/ZnSe heteronanostructure arrays give rise to excellent visible light driven photocatalytic activities for degradation of RhB, much superior than that of ZnO-NRs array by the enhanced visible light absorption of ZnSe nanostructures and effective separation of the photoinduced electron-hole pairs by the coupling effect of the ZnO-NRs/ZnSe heteronanostructures. Moreover, the outstanding photocatalytic recycled stability of the heteronanostructure array makes it a remarkably promising candidate for solar-driven photocatalytic applications.

Acknowledgments

The authors thank the Natural Science Foundation of China (21201007 and 21271009) and the Program for New Century Excellent Talents in University (NCET 11–0888) for financial support.

Notes and references

Anhui Key Laboratory of Molecule-Based Materials, The Key Laboratory of Functional Molecular Solids, Ministry of Education, Center of nano science and technology, College of Chemistry and Materials Science, Anhui Normal University, Wuhu 241000 (P. R. China)
Fax: +86 553 3869303; Tel: +86 553 3869303; E-mail: zhengcui@mail.ahnu.edu.cn (Z. Wu); bygeng@mail.ahnu.edu.cn (B. Geng).

† Electronic Supplementary Information (ESI) available: See DOI: 10.1039/b000000x/.

1 T. Clasen and P. Edmondson, *Int. J. Hyg. Environ. Health* 2006, **209**, 173–181.
2 G. Palmisano, V. Augugliaro, M. Pagliaro and L. Palmisano, *Chem. Commun.* 2007, **43**, 3425–3437.
3 C. C. Chen, W. H. Ma, J. C. Zhao, *Chem. Soc. Rev.* 2010, **39**, 4206–4219.
4 Q. P. Luo, B. X. Lei, X. Y.Yu, D. B. Kuang and C. Y. Su, *J. Mater. Chem.* 2011, **21**, 8709–8714.
5 Y. S. Kim and S. H. Kang, *Nanotechnology* 2011, **22**, 275707.
6 Y. Hong, C. G. Tian, B. J. Jiang, A. P. Wu, Q. Zhang, G. H. Tian and H. G. Fu. *J. Mater. Chem. A* 2013, **1**, 5700–5708.
7 (a) J. Ryu, W. Choi, *Environ. Sci. Technol.* 2004, **38**, 2928–2933. (b) H. B. Zeng, W. P. Cai, P. S. Liu, X. X. Xu, H. J. Zhou, C. Klingshirn, H. Kalt, *ACS Nano* 2008, **2**, 1661–1670.
8 D. Robert, *Catal. Today* 2007, **122**, 20–26.
9 N. Helaïli, Y. Bessekhouad, A. Bouguelia and M. Trari, *Sol. Energy* 2010, **84**, 1187–1192.
10 Y. X. Liu, J. X. Shi, Q. Peng and Y. D. Li, *Chem. Eur. J.* 2013, **19**, 4319–4326.
11 M. Basu, N. Garga and A. K. Ganguli, J. *Mater. Chem. A* 2014, **2**,

7517–7525.
12 S. S. Ma, J. J. Xue, Y. M. Zhou and Z. W. Zhang, *J. Mater. Chem. A* 2014, **2**, 7272–7280.
13 S. Khanchandani, S. Kundu, A. Patra and A. K. Ganguli, *J. Phys. Chem. C* 2012, **116**, 23653−23662.
14 K. S. Leschkies, R. Divakar, J. Basu, E. Enache-Pommer, J. E. Boercker, C. B. Carter, U. R. Kortshagen, D. J. Norris and E. S. Aydil, *Nano Lett.* 2007, **7**, 1793−1798.
15 X. Cao, P. Chen and Y. Guo, *J. Phys. Chem. C* 2008, **112**, 20560−20566.
16 (a) K. Wang, J. J. Chen, W. L. Zhou, Y. Zhang, Y. F. Yan, J. Pern and A. Mascarenhas, *Adv. Mater.* 2008, **20**, 3248–3253. (b) Z. M. Wu, Y. Zhang, J. J. Zheng, X. G. Lin, X. H. Chen, B. W. Huang, H. Q. Wang, K. Huang, S. P. Li and J. Y. Kang, *J. Mater. Chem.* 2011, **21**, 6020–6026. (c) S. Cho, J. W. Jang, S. H. Lim, H. J. Kang, S. W. Rhee, J. S. Lee and K. H. Lee, *J. Mater. Chem.* 2011, **21**, 17816–17822. (d) L. L. Chen, W. X. Zhang, C. Feng, Z. H. Yang and Y. M. Yang, *Ind. Eng. Chem. Res.* 2012, **51**, 4208−4214. (e) S. Cho, J. W. Jang, J. S. Lee and K. H. Lee, *Nanoscale* 2012, **4**, 2066–2071. (f) S. Cho, J. W. Jang, J. Kim, J. S. Lee, W. Choi and K. H. Lee, *Langmuir* 2011, **27**, 10243–10250. (g) M. Y. Chen and Y. J. Hsu, *Nanoscale* 2013, **5**, 363–368.
17 Z. C. Wu, C. R. Xu, Y. Q. Wu, H. Yu, Y. Tao, H. Wan and F. Gao, *CrystEngComm* 2013, **15**, 5994−6002.
18 Z. C. Wu, Y. Q. Wu, T. H. Pei, H. Wang and B. Y. Geng, *Nanoscale* 2014, **6**, 2738−2745.
19 H. Kaneka, S. Nishimoto, K. Miyake and N. Suedomi, *J. Appl. Phys.* 1986, **59**, 2526–2534.
20 S. J. Hong, S. Lee, J. S. Jang and J. S. Lee, *Energy Environ. Sci.* 2011, **4**, 1781–1787.
21 J. W. Tang, Z. G. Zou and J. H. Ye, *J. Phys. Chem. B* 2003, **107**, 14265−14269.
22 Y. F. Sun, B. Y. Qu, Q. Liu, S. Gao, Z. X. Yan, W. S. Yan, B. C. Pan, S. Q. Wei and Y. Xie, *Nanoscale* 2012, **4**, 3761−3767.
23 V. Fischer, M. B. Bannwarth, G. Jakob, K. Landfester and R. Muñoz-Espí, *J. Phys. Chem. C* 2013, **117**, 5999−6005.
24 Y. Liu, L. Yu, Y. Hu, C. F. Guo, F. M. Zhang and X. W. Lou, *Nanoscale* 2012, **4**, 183−187.
25 F. Song, X. L. Hu, *Nat. Commun.* 2014, **5**, 4477.
26 Y.-S. Hu, A. Kleiman-Shwarsctein, A. J. Forman, D. Hazen, J.-N. Park and E. W. McFarland, *Chem. Mater.* 2008, **20**, 3803–3805.
27 L. Q. Ye, L. Zan, L. H. Tian, T. Y. Peng and J. J. Zhang, *Chem. Commun.* 2011, **47**, 6951−6953.
28 J. C. Zhao, T. X. Wu, K. Q. Wu, K. Oikawa, H. Hidaka and N. Serpone, *Environ. Sci. Technol.* 1998, **32**, 2394−2400.
29 T. X. Wu, G. M. Liu, J. C. Zhao, H. Hidaka and N. Serpone, *J. Phys. Chem. B* 1998, **102**, 5845−5851.
30 M. L. Guan, C. Xiao, J. Zhang, S. J. Fan, R. An, Q. M. Cheng, J. F. Xie, M. Zhou, B. J. Ye and Y. Xie, *J. Am. Chem. Soc.* 2013, **135**, 10411−10417.
31 S. Cho, J. W. Jang, J. S. Lee and K. H. Lee, *Nanoscale* 2012, **4**, 2066–2071.

Graphical Abstract

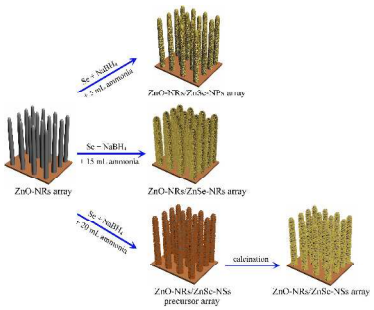

The high visible light photocatalytic activity of ZnO naorods/ZnSe heteronanostructure arrays with a tunable microstructure of ZnSe shell are achieved by the liquid chemical conversion with ZnO nanorods array on zinc foil.